©2015 Society of Economic Geologists, Inc.
Economic Geology, v. 110, pp. 2025–2040

The Age of the Latest Thermal Overprint of Tin and Polymetallic Deposits in the Erzgebirge, Germany: Constraints from Fluorite (U-Th-Sm)/He Thermochronology*

R. Wolff,[1,†] I. Dunkl,[1] U. Kempe,[2] and H. von Eynatten[1]

[1] *University of Goettingen, Geoscience Center, Sedimentology and Environmental Geology, Goldschmidtstr. 3, 37077 Goettingen, Germany*

[2] *TU Bergakademie Freiberg, Institut für Mineralogie, Brennhausgasse 14, 09596 Freiberg, Germany*

Abstract

The Erzgebirge region of Germany records two major episodes of hydrothermal activity, which includes a Late Carboniferous to Early Permian event associated with significant Sn-W mineralization that is related to late Variscan granite magmatism, and a Mesozoic episode of polymetallic vein mineralization. In contrast to the first event, the age of the younger hydrothermal activity is poorly constrained. For the latter, various geochronological methods yielded a wide age range from Permian to early Tertiary. Here we apply fluorite (U-Th-Sm)/He thermochronology (FHe) on both types of mineralization with a twofold goal: (1) to investigate the sensitivity and applicability of the new FHe method (Evans et al., 2005), and (2) to constrain the thermal history of ore deposits in the Erzgebirge region. Two hundred and thirty-three aliquots from seven mineralization localities have been dated. Fluorite from six deposits yielded Cretaceous FHe ages between 112 to 79 Ma, which are independent of their paragenesis. In contrast, fluorite from the Sadisdorf Sn-W deposit yielded an age of 234 Ma. The younger ages are interpreted as cooling ages indicating the time of the last thermal overprint, including possible hydrothermal activity, in the Erzgebirge. The oldest, Triassic FHe ages at Sadisdorf indicate that the Mesozoic thermal overprint only partially reset the (U-Th-Sm)/He system of the late Variscan mineralization. Thermal modeling based on FHe ages and He diffusion parameters in fluorite results in thermal histories comparable to the results from the well-established apatite-based thermal modeling. This study emphasizes the applicability of fluorite (U-Th-Sm)/He thermochronology, which is especially suited for ore deposits where apatite is lacking.

Introduction

Fluorite is a mineral commonly occurring (1) in hydrothermal deposits; (2) as an accessory phase in granites, pegmatites, carbonatites, and alkaline magmatites; (3) in stratabound ore deposits; and (4) as authigenic phase in sandstones. In particular, hydrothermal veins occur in a wide range of geologic settings, which are not all well suited for the commonly used apatite thermochronology because apatite easily dissolves in the presence of acid fluids. The need to determine the age of such ore deposits has led to the development of isotopic techniques for fluorite geochronology such as the Sm/Nd (Chesley et al., 1991, 1994) and U-Th-Pb methods (Hofstra et al., 2000). Fluorite low-temperature thermochronology using the fission track technique was first attempted by Grønlie et al. (1990). Recently, the fluorite (U-Th-Sm)/He method (FHe) was introduced by Evans et al. (2005) and applied by Pi et al. (2005) and Siebel et al. (2010). According to these studies, the closure temperature of the (U-Th-Sm)/He fluorite system ranges between ca. 170° and 60°C (Evans et al., 2005; Pi et al., 2005), which is well suited for dating low-temperature thermal and hydrothermal events. To investigate the sensitivity and routine applicability of FHe thermochronology, we have performed a comprehensive study on fluorite from several ore deposits in the Erzgebirge (German ore mountains; Fig. 1). The Erzgebirge is an ideal test area because it hosts numerous well-studied ore deposits of variable types often containing fluorite (e.g., Kempe et al., 2002). Moreover, the complex post-Variscan thermal history of the Erzgebirge is extensively studied by K-Ar and Ar-Ar studies on mica and hornblende (Werner and Lippolt, 2000), apatite fission track analysis (Ventura and Lisker, 2003; Lange et al., 2008), as well as zircon and apatite (U-Th-Sm)/He thermochronology (Wolff et al., 2015). These studies suggest a significant Mesozoic sedimentary burial after the post-Variscan denundation and before the Variscan basement has been reexhumed in the Late Cretaceous (Voigt, 2009). This thermal history is superimposed by hydrothermal activity. Our study, performed on fluorite from various sites in the Erzgebirge, demonstrates that FHe thermochronology serves as an excellent tool to constrain the minimum age of the latest thermal overprint in such a complex ore district.

Regional Geology and Post-Variscan Tectonic Evolution

The Erzgebirge forms an antiform structure exposing high- to medium-grade metamorphic gneisses in the core surrounded by a sequence of low-grade metamorphic units, mainly composed of micaschists and phyllites. This metamorphic assemblage formed by crustal stacking during the Carboniferous (e.g., Werner and Lippolt, 2000) and was later intruded by late- to post-Variscan granitoids and locally covered by rhyolites (Kossmat, 1925; Romer et al., 2007; see Fig. 1b). The Erzgebirge is bordered in the east by the Lausitz thrust to the Cadomian basement of the Lausitz block (Linnemann and Romer, 2002). This fault is sealed by Cretaceous deposits that formed at the margin of the synsedimentary uplifting block in the east. The initially flexural margin was later transformed into a thrust (Linnemann and Romer, 2010). The Eger fault delimits the Erzgebirge toward the south (e.g., Kroner et al., 2007; Fig. 1b). The post-Variscan

† Corresponding author: e-mail, rwolff@gwdg.de

*Electronic Appendices to this paper is available at http://economicgeology.org/ and at http://econgeol.geoscienceworld.org/.

0361-0128/15/4358/2025-16

Submitted: March 3, 2015
Accepted: June 9, 2015

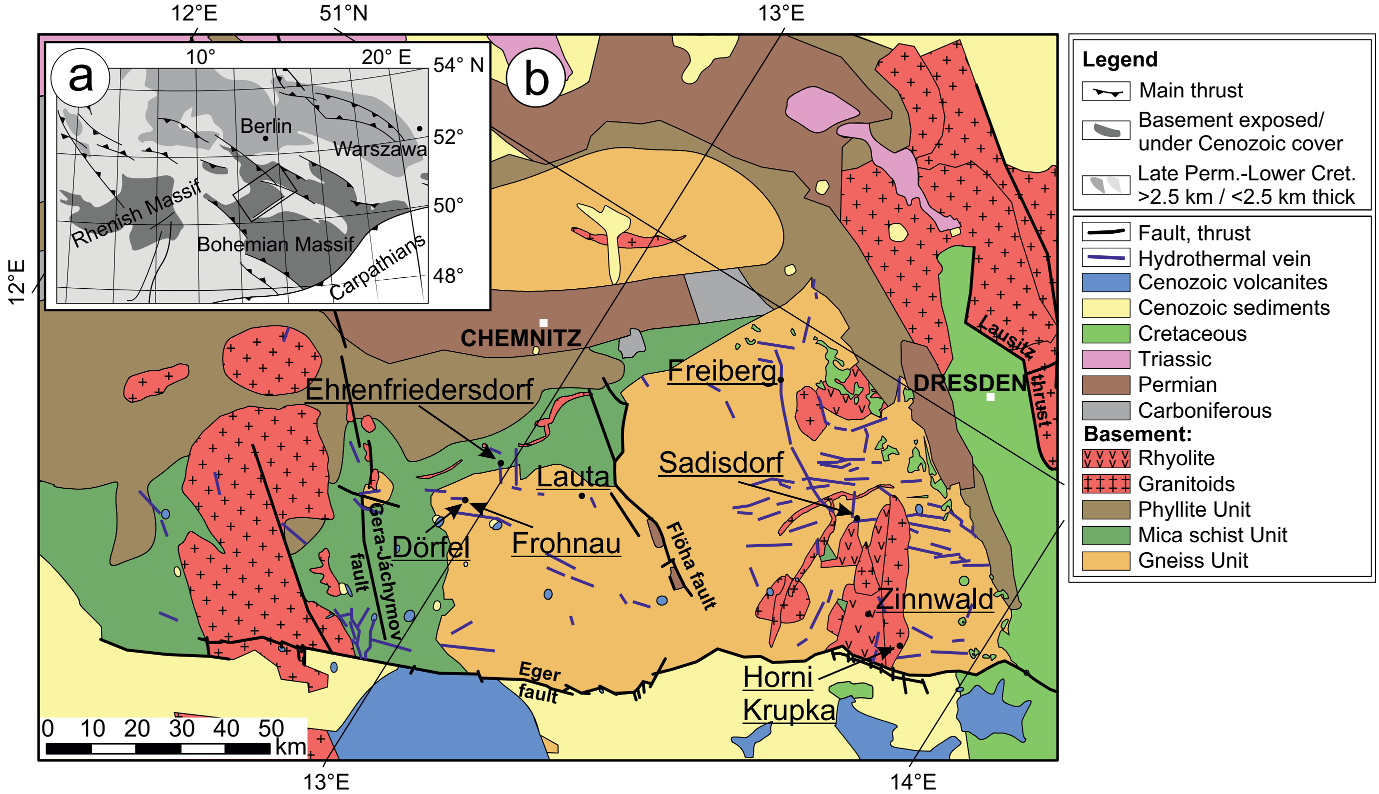

FIG. 1. (a). Position of the Erzgebirge (German ore mountains) in the European Variscides and surrounding Permo-Mesozoic basins (modified after Kley, 2013). Rectangle represents the position of the study area. (b). Geologic map of the Erzgebirge (simplified after Wolf et al., 1992) with sample locations (underlined) and major fault zones.

sedimentary cover of the region starts with Late Carboniferous to Early Permian continental deposits. In the Triassic, the area formed a marginal part of the Central European basin and experienced some subsidence, as suggested by facies and thickness trends from surrounding Triassic deposits (Voigt, 1995). West, north, and east of the Erzgebirge, the Permian to Triassic sequences are still preserved (Fig. 1a), but the thickness of the former cover on the currently exposed Erzgebirge is a matter of debate (Schröder, 1976; Brause, 1988; Götze, 1998; Voigt, 2009). Schröder (1987) estimates a thickness of 1.5 km, while Dudek et al. (1991) postulates a post-Variscan denudation of at least 2.5 km. Thermal modeling reveals a Permo-Mesozoic burial temperature reaching ca. 80° to 100°C at the south, while the sedimentary cover thins out toward the north (Wolff et al., 2015).

In the eastern Erzgebirge, Upper Cretaceous (Cenomanian to Coniacian) sediments transgressively overlie the Variscan basement (e.g., Pietzsch, 1913; Kossmat, 1925; Wolf et al., 1992; Prazak, 1994; Voigt, 1995; Janetschke and Wilmsen, 2014). In the Middle Cenomanian, the Niederschöna paleoriver delivered sediments into the northern part of the Bohemian Cretaceous basin (Kossmat, 1925; Voigt, 1998; Schröder and Peterek, 2001; Voigt, 2009). Gravel composition reveals that during this time, the Triassic sedimentary cover has already been removed. Final exhumation of the Erzgebirge and the entire northern Bohemian massif in the late Cenozoic has led to almost complete denudation of the Upper Cretaceous sedimentary cover. Sedimentary data (Voigt, 2009) and cooling ages of the Lausitz massif (Lange et al., 2008) reveal exhumation exceeding at least 4 km during Late Cretaceous basin inversion (Voigt, 2009). In adjacent areas, similar amounts of Late Cretaceous inversion have been reported, for instance, from the Karkonosze and Harz mountains, and Thuringian forest (Thomson and Zeh, 2000; von Eynatten et al., 2008; Danišík et al., 2010).

In the western Erzgebirge the basement is partly covered by Eocene to Oligocene fluvial deposits (Knobloch et al., 1996) and locally by Oligocene and lower Miocene mafic lava flows (Suhr, 2003). The lavas originally flowed in paleovalleys, but now they are forming elongated hills representing the Neogene palaeosurface. Locally the relief inversion allows estimating the post-Eocene erosion to be less than 200 m (Eissmann, 1997). However, Ventura and Lisker (2003) suggested a late Cenozoic denudation that removed a thick cover layer (2.1–5.6 km) connected to the activity of the Eger graben in the Oligocene. This eroded thickness is debated. For instance, according to their apatite fission track data Lange et al. (2008) favored less than 1 km for late Cenozoic denudation. The minor Cenozoic denudation is also supported by the apatite (U-Th)/He thermochronological data of Wolff et al. (2015).

Hydrothermal Activity and Vein Ore Deposits

The Erzgebirge is famous for its numerous vein ore deposits which have been extensively mined for centuries. There is a complex picture of relationships between Variscan magmatism, tectonic setting, vein composition, and the ore type for various mineralization sequences (W, Sn-W, Zn-Pb-Cu, Ag-Sb, Bi-Co-Ni-U, etc.). Accordingly, there is a long-lasting debate on the genesis and timing of various types of mineralizations. Recently, two major periods of hydrothermal activity are commonly distinguished. The first is related to late Variscan granitoid magmatism, the second is assumed to be Mesozoic (Fig. 2a; Baumann et al., 2000; Seifert, 2008; Romer et al., 2010b). There are, however, conflicting views assuming that the second period is also late Variscan (e.g., Tischendorf et al., 1989). Depending on the approach used in various studies (with the mineral association, tectonic position, and/or relative age relationships as the main classification criteria), mineralization styles were assigned alternatively to the late Variscan or to the Mesozoic period (Baumann, 1967, 1994a, b; Tischendorf, 1989; Höhndorf et al., 1994; Kuschka, 1996, 1997; Baumann et al., 2000; Seifert, 2008). Furthermore, mineralization types belonging to different styles and periods may be superimposed within one single vein system as may be illustrated by the Ehrenfriedersdorf tin deposit investigated in more detail in this work (Hösel et al., 1994; Kumann and Leeder, 1994). There is, however, a consensus that (1) the typical Sn-W mineralization belongs to the first, late Variscan period and (2) the characteristic polymetallic or fluorite-barite mineralization (so-called "fba") belongs to the second, post-Variscan period (referred to as "Mesozoic" in this work).

Early applications of isotope geochronology (pitchblende chemical U-Pb and Pb/Pb dating and K-Ar dating on altered wall rocks; see review by Baumann, 1967) indicated two main events of late Variscan and Mesozoic (180–80 Ma) ages, and a multiple remobilization of uranium in the related deposits starting from the late Variscan. The latter phenomenon was confirmed by more recent studies (Eikenberg, 1991; Förster and Haack, 1996).

The late Variscan emplacement of granitoids, rhyolites, and lamprophyric dikes was accompanied by increased high-T hydrothermal activity and associated with Sn-W and Mo enrichment in greisen, vein, and skarn deposits (e.g., Stemprok and Sulcek, 1969; Baumann et al., 2000; Dolejs and Štemprok, 2001; Seifert, 2008; Romer et al., 2010a). The age of this early mineralization is now well constrained to a time interval between Late Carboniferous to Early Permian (e.g., Tischendorf and Förster, 1990; Baumann et al., 2000). Nevertheless, exact absolute age relationships between magmatism and ore precipitation are a matter of considerable debates. For example, a Carboniferous or Permian age of tin mineralization is highly controversial (Kempe et al., 2004; Romer et al., 2007, 2010a).

The Mesozoic mineral veins are predominantly polymetallic of barite-fluorite-sulfide and hematite-barite type hosted in the metamorphic basement rocks. Some veins contain anomalous concentrations of U, Ba-Sr, Bi-Co-Ni-As-Ag, and Ge-Hg or Fe-Mn (e.g., Trinkler et al., 2005; Seifert, 2008). This second ore formation period may have been driven by major tectonic events affecting the European continent, such as the Triassic opening of the Tethys or Jurassic to the Cretaceous opening of the Central and North Atlantic (Mitchell and Halliday, 1976; Halliday and Mitchell, 1984; Cathelineau et al., 1990; Baumann and Weber, 1996; Romer et al., 2010b). Tischendorf and Förster (1990) related the late vein-type

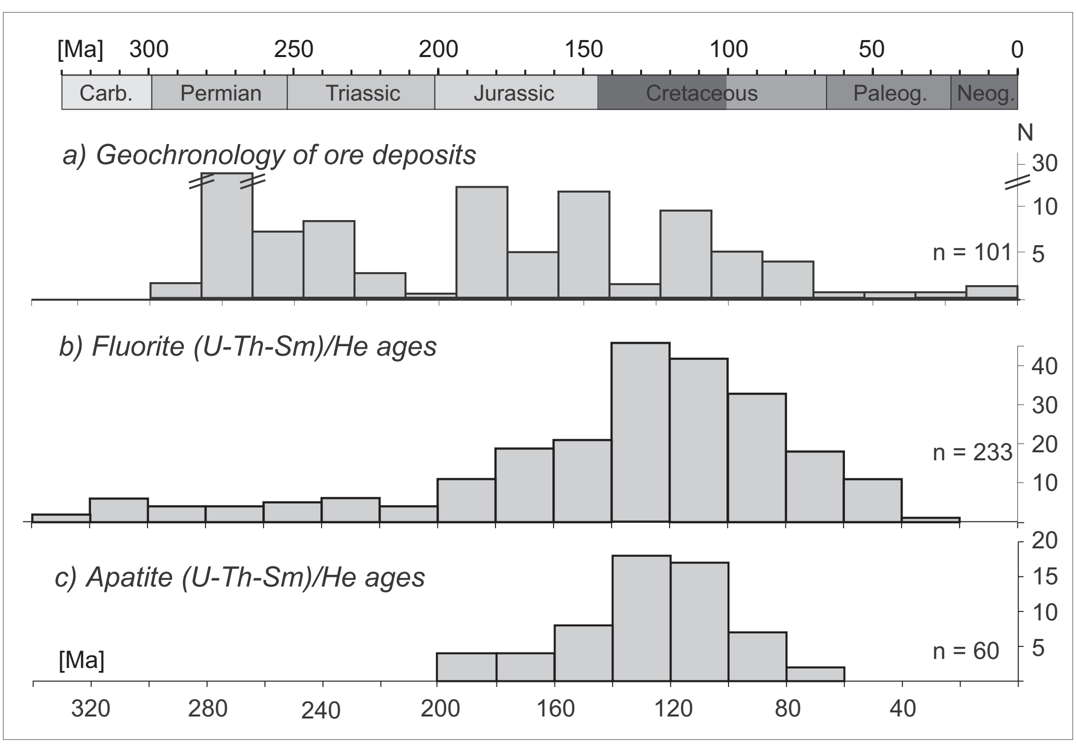

FIG. 2. (a). Compilation of geochronological data from the literature, indicating a broad and diffuse age range from Permian to Tertiary for hydrothermal activity in the Erzgebirge (pitchblende U-Pb (mostly 260–280 Ma), muscovite and feldspar K-Ar and Rb-Sr, fluorite Sm-Nd, and sphalerite Rb-Sr ages; Lower and Upper Cretaceous are subdivided; from Romer et al., 2010b); (b). Fluorite (U-Th-Sm)/He thermochronological data (this work). (c). AHe ages from Wolff et al. (2015).

deposits to the Alpine orogenesis that had a remote influence on the European Variscides. The relative age relationships of the Mesozoic vein systems are studied in detail by Seifert et al. (1992), Baumann (1994a, b), Kuschka (1996, 1997), Baumann et al. (2000), and Seifert (2008) and were recently reviewed by Romer et al. (2010b). The age of the second period is still poorly constrained and assigned mostly to the Mesozoic by recent workers (e.g., Höhndorf et al., 1994; Trinkler et al., 2005; Romer et al., 2010b; Fig. 2a). According to Klemm (1994), fluids from polymetallic mineralizations show chemical compositions typical of brines in deeply buried sedimentary basins.

Sampling and Methods

We focused our study on fluorite samples from the two well-defined mineralization types: from the late Variscan Sn-W and from the Mesozoic polymetallic deposits (so-called "fba-type" with fluorite and barite). Samples from Sn-W deposits were collected mainly from underground mines and from open pits (Horni Krupka, Zinnwald, Sadisdorf, Ehrenfriedersdorf, and Dörfel). Most of them were characterized in more details previously (Kempe et al., 2002; Monecke et al., 2011). Additional samples were collected from mine dumps and received from museums in Dörfel, Zinnwald, and Ehrenfriedersdorf (Fig. 1b, Table 1). These samples belong mainly to the late Variscan Sn-W mineralization. However, samples from Mesozoic mineralizations, which are also present at Ehrenfriedersdorf and Dörfel, were studied as well. The fluorite associated with Sn-W mineralization is well characterized by specific rare earth element (REE) patterns displaying distinct negative and positive Eu anomalies, enrichment of heavy REEs, and often also the tetrad effect (Monecke et al., 2002, 2011). Fluorite samples from Mesozoic polymetallic deposits (Freiberg, Lauta, and Frohnau) were collected from mine dumps or obtained from museum collections. Fluorite of this type is often characterized by a conspicuous yellow to honey-brown color. Such typical color often occurs together with violet or greenish color in single fluorite crystals or aggregates.

TABLE 1. Summary of the Obtained Fluorite (U-Th-Sm)/He Ages, Sample Locations, and REE + Y Content of the Studied Fluorite Samples from the Erzgebirge

				Sample-average FHe data					Locality-average FHe data		
Locality	Samples	Lat. (° North)	Long. (° East)	Number of ages	Median (Ma)	CI (Ma)	REE+Y (ppm)	Color	Number of ages	Median (Ma)	CI (Ma)
Annaberg Dörfel	RW-2-12	50.5765	12.9525	9	99.2	21.7	563	Yellow	42	104.5	7.4
	RW-2-15a			8	179.4	34.4	276	Colorless			
	RW-2-15b			11	123.9	13.8	227	Green			
	RW-2-15c			5	69.3	19.1	259	Pink			
	RW-2-15d			9	84.0	8.1	398	Pink			
	DF15			--	--	--	62	Colorless			
Annaberg Frohnau	FRO-1	50.5765	12.9525	11	98.9	10.7	614	Colorless	30	80.6	9.2
	RW-2-23a			3	60.0	--	337	Colorless			
	RW-2-23b			2	48.0	--	221	Black			
	RW-5-25a			5	75.3	8.8	440	Honey			
	RW-5-25b			4	42.3	76.1	168	Pink			
	RW-9-8a			5	93.0	19.0	156	Yellow			
Ehrenfriedersdorf	ED268	50.6418	12.9789	4	122.1	24.6	273	Rosa	54	109.7	4.5
	ED506			1	101.9	--	--	Pink			
	RW-2-20			15	118.2	8.9	424	Yellow			
	RW-2-21			8	119.9	15.0	401	Honey			
	RW-2-22a			9	110.4	4.8	370	Pink			
	RW-2-22b			13	95.4	10.7	325	Pink			
	RW-9-5			4	89.2	31.0	343	Yellow			
Freiberg	RW-9-1	50.9598	13.0023	--	--	--	436	Honey	--	--	---
	RW-9-12b			--	--	--	535	Yellow			
	RW-9-13			--	--	--	72	Colorless			
Horni Krupka	RW-5-7	50.7165	13.8550	1	36.5	--	125	Colorless	19	79.0	10.4
	RW-5-8			8	79.0	6.6	126	Colorless			
	RW-5-9			6	101.7	7.0	1353	Honey			
	RW-5-10			4	22.5	4.2	224	Colorless			
Lauta	RW-2-8a	50.6634	13.1543	11	74.7	7.4	510	Honey	35	111.7	10.3
	RW-2-8b			6	113.5	32.4	329	Pink			
	RW-2-8c			9	133.9	21.7	388	Pink			
	RW-2-8d			9	164.5	42.5	251	Black			
Sadisdorf	SD41	50.8251	13.6463	3	215.7	--	2514	Colorless	20	234.4	15.9
	SD1001			9	228.3	19.2	502	Brown			
	SD1004b			4	293.3	19.7	883	Brown			
	UK86			4	210.9	31.2	222	Colorless			
Zinnwald	RW-5-11	50.7294	13.7675	10	76.3	18.6	116	Black	33	109.7	10.1
	ZW1005			4	71.0	23.9	1382	Green			
	ZW315/2g			17	130.7	10.6	1854	Green			
	ZW322			2	86.4	--	46	Pink			

Notes: The confidence interval (CI) of the median is calculated according to Bonett and Price (2002); -- = no information

Moreover, such Mesozoic polymetallic fluorites are typified by a hump-shaped REE distribution pattern with an enrichment of the middle REE and weak Eu anomalies (Trinkler et al., 2005). The characteristics described above may be used as a criterion to distinguish late Variscan Sn-W and Mesozoic polymetallic samples when various fluorite types are present in a single deposit. To cover the full scale of specific fluorite types, samples covering a broad variety of colors have been selected from each locality. All samples investigated are listed in the electronic Appendix 1.

Fluorite samples from Horni Krupka, Ehrenfriedersdorf, Dörfl, Frohnau, and Lauta were studied by cathodoluminescence (CL) imaging and spectroscopy to check their defect structure, homogeneity, and internal textures (cf. Kempe and Götze, 2002) if not previously investigated (Kempe et al., 2002). For CL imaging, a JEOL scanning electron microscope (SEM) JSM 7001F with a thermal field emission electron gun equipped with a GATAN MiniCL detector was used. For picture photographs, the SEM was operated at 20 kV and 0.6 nA. CL spectra were obtained by means of a system consisting of a GATAN MonoCL 4 mirror, an optical fiber guide, and a Princeton Instruments monochromator Acton SP 2300 equipped with a PIXIS 256 CCD which was attached to the same microscope. The SEM was operated at 20 kV and 1nA with a defocused beam when taking the spectra.

Fluorite (U-Th-Sm)/He thermochronology was performed on 233 aliquots of 38 samples (between 1 and 17 aliquots/sample; Table 1) from eight localities (see details in electronic App. 1). In the samples from the Freiberg mining district and from the Sn-bearing veins at Dörfel, the measured He content was too low to obtain meaningful results. Thus, these samples are not considered for age interpretations. For sample preparation, the outer surface of the euhedral crystals was stained by a marker pen and afterward carefully crushed. Only intact shards derived from the interior of the crystals with no or only very tiny inclusions were selected to avoid implantation of helium from U-Th-Sm-rich phases and alpha ejection as well as excess He and tiny mineral phases of extreme actinide content (cf. Pi et al., 2005; Fig. 3). Typically, an average fragment size of ca. 100- to 400-μm edge length was used. The alpha-ejection correction (Farley et al., 1996) was not necessary in this case because fragments from the outer surface of the crystals were excluded. Only single-fragment aliquots were dated. The rationale behind this analytical concept was to study the reliability of the method when the dated volumes are very small in size and might be influenced by primary or secondary zoning that is common in fluorite crystals (e.g., Kempe et al., 2002; Schwinn and Markl, 2005). Furthermore, such heterogeneity may also be related to a possible age distribution within the samples, which would be overlooked if larger sample sizes are used for analysis as discussed below. Furthermore, the accumulation of helium may be spatially decoupled from the volumes where the alpha-emitting elements are concentrated, which could have remarkable effects in zoned crystals due to the travel range of alpha particles, which is ca. 13 to 14 μm for ^{238}U and ^{232}Th in fluorite (calculated by the SRIM method, see Ziegler et al., 2010). Multifragment aliquots may yield more consistent ages as in this way the randomly biased fragments average the influence of alpha ejection and other factors (see discussion below).

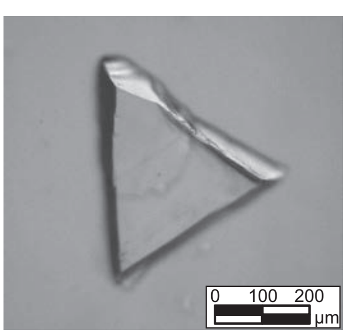

FIG. 3. Image of a typical single fluorite fragment analyzed (inclusion-free, photographed in ethyl alcohol).

The single-fragment aliquots were wrapped in ca. 1 × 1-mm-sized platinum capsules and degassed in high vacuum by heating with an infrared diode laser. The extracted gas was purified using a SAES Ti-Zr getter at 450°C. The chemically inert noble gases and a minor amount of other rest gases were then expanded into a Hiden triple-filter quadrupole mass spectrometer equipped with a positive ion counting detector. Crystals were checked for complete degassing of helium by sequential reheating and helium measurement. Following degassing, samples were retrieved from the gas extraction line, unpacked and spiked with calibrated ^{230}Th and ^{233}U solutions. The fluorites were then dissolved in Savillex Teflon® vials using ultrapure 30 % HCl at 75°C and held for 24 h at this temperature until total drying. The digestion was controlled by a stereo microscope and the last step was repeated until total dissolution. The sample solutions were analyzed in 4% HCl matrix, using a Perkin Elmer Elan DRC II ICP-MS equipped with an APEX microflow nebulizer. The actinide concentrations were determined by isotope dilution method and the Sm and the other REEs by external calibration method. The level of detections was between 1 and 2 pg, slightly varying for the different ICP-MS sessions. FHe ages were calculated using Taylor series that can be summarized by

$$^{4}He_t = {}^{4}He_i + 8*^{238}U(\exp^{(\lambda 238t)} - 1) + 7*^{235}U(\exp^{(\lambda 235t)} - 1) + 6*^{232}Th(\exp^{(\lambda 232t)} - 1) + {}^{147}Sm(\exp^{(\lambda 147t)} - 1),$$

where $^{4}He_t$ and $^{4}He_i$ are the total and initial helium content, respectively (McDougall and Harrison, 1988). The uncertainties of FHe ages were calculated as a square root of the sum of squares of uncertainty of He and He-production-weighted uncertainties of U, Th, and Sm measurements. The sample and locality averages are expressed—to a first approximation—as medians because the single-fragment ages are mostly not Gaussian distributed and thus the arithmetic mean and the standard deviation are not statistically robust (see discussion below). For the same reason we cannot apply any standard deviation-based outlier rejection procedure like that suggested by Fitzgerald et al. (2006) for apatite (U-Th)/He data. Remarkably, the analytical uncertainties of He and actinide data do not provide hints for rejection of individual ages that are considerably older than the dominant proportion of age data.

The concentrations of REEs and some other elements were determined on the dissolved crystal fragments that were used for (U-Th-Sm)/He geochronology. Fluorites with an REE + Y content exceeding 3,000 ppm have been excluded from this study to avoid extreme chemical compositions which may change significantly the diffusion mechanisms and thus influence the closure temperature (T_c) of fluorite.

Results

Cathodoluminescence (CL)

CL imaging and spectroscopy demonstrate a significant heterogeneity in the defect structure of fluorite crystals and aggregates from Mesozoic polymetallic or fluorite-barite veins in accordance with earlier results obtained for the samples from late Variscan Sn-W mineralization (Kempe et al., 2002). This heterogeneity is only partly paralleled by visible variations in color. The imaged textures may be related to primary growth zoning (oscillatory zoning, sector zoning, etc.) and secondary alteration, respectively. This is illustrated by the fluorite-barite vein sample RW-2-22a from Ehrenfriedersdorf in Figure 4a, b. This sample is mainly transparent and exhibits a yellow to honey-brown color with some cloudy patchy violet inner and normally zoned violet outer rim zones and a few small, nearly colorless crystal overgrowths (Fig. 4a). The cloudy patchy violet zones are clearly related to secondary alteration. In CL images, the yellow to honey-brown crystal parts appear dark or weakly luminescent with normal oscillatory and sector growth zoning. The weak luminescence is mainly related to the emission lines from $REE^{3+/2+}$ centers and a broadband feature peaking at about 575 nm (Fig. 4b). The luminescence of cubic Dy^{3+} at 671 and 759 nm prevails over noncubic Dy^{3+} (482 and 584 nm) in accordance with the dilute character of the incorporation of the REEs. In contrast, the cloudy violet patches exhibit strong luminescence (Fig. 4a) dominated by two broadband features peaking at 305 and 565 nm, respectively (Fig. 4b). Luminescence signals from REEs (Eu^{2+} and noncubic Dy^{3+}) are only of very minor importance in these spectra. The band shape of the main luminescence features and comparison with the spectra of the yellow crystal parts indicate that the bands at 305 and 575 nm consist of more than one signal. The nature of these bands is

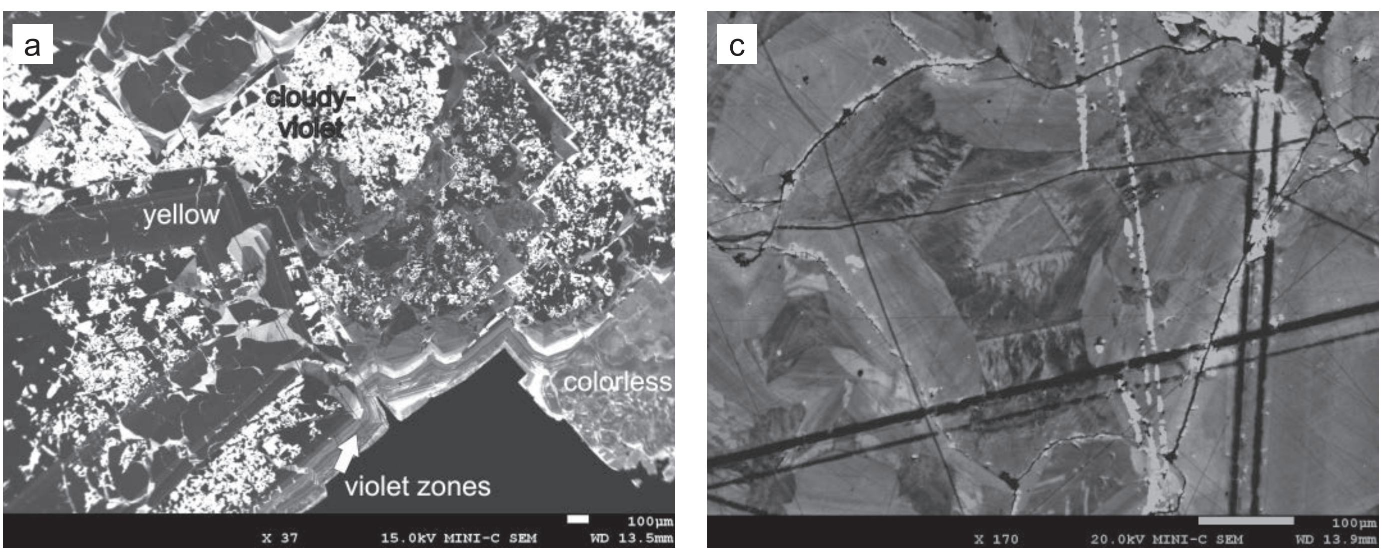

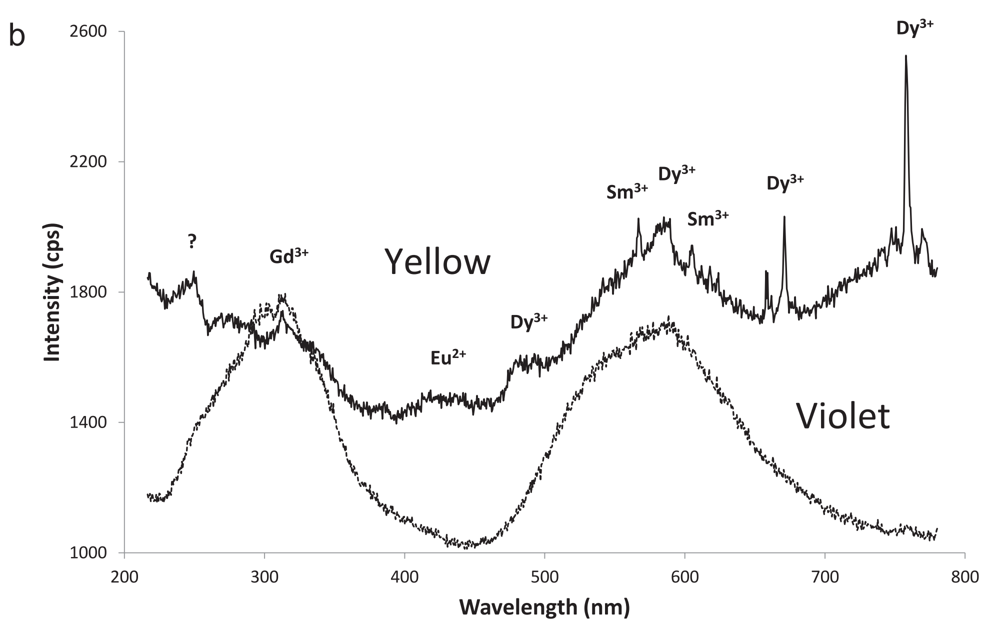

FIG. 4. SEM-CL images and spectra of fluorite from Mesozoic ("fba") mineralization: (a). CL image of fluorite sample RW-2-22a (Ehrenfriedersdorf) with yellow to honey-brown central crystal parts infiltrated by violet patchy zones of secondary alteration. An almost colorless overgrowth is visible in the lower right part of the image. Note that outer crystal rims also contain some violet zones (arrow). (b). Typical CL spectra from (a) of a weak luminescent yellow and strongly luminescent patchy violet crystal part. The spectra are stacked for clarity. See text for further explanations. (c). CL image of fluorite sample RW-2-8c (Lauta) with primary oscillatory and sector zoning. Note the fibrous internal texture of the violet colored crystal sectors.

unclear. Investigation on pure, artificially grown optical fluorite indicates that they are related to the concentration of interstitial defects occurring in variable amounts depending on growth conditions (Kempe et al., unpub. data). In contrast, violet zones in oscillatory growth zoning are characterized by very low luminescence intensity (Fig. 4a). We assume that such zones formed during circulation of U-rich fluids (Kempe et al., 2002) but the zones are often not enriched in uranium. A characteristic feature of them is a fibrous internal texture illustrated here by CL imaging of a sample from Lauta (RW-2-8c; Fig. 4c). All described types of defect structures enhancing, modifying, or quenching CL emission may also influence the He diffusion behavior in fluorite and thus the ability of the structure to retain He. It is not possible to separate the various fluorite types from each other by handpicking without CL imaging.

REE contents

The average REE + Y content of the 233 dated fluorite aliquots is 479 ppm (details in electronic App. 1). The results of the REE measurements are presented in REE patterns obtained by chondrite normalization using the values by Sun and McDonough (1989). The patterns can be subdivided into two major groups according to the two mineralization types to which they belong (Fig. 5). The samples from Lauta, Frohnau, and Freiberg show mainly hump-shaped patterns (i.e., mid-REE enrichment) with minor Eu anomalies, which is typical for the Mesozoic fluorite-barite deposits. In contrast, samples from Zinnwald, Horni Krupka, and Sadisdorf display pronounced Eu anomalies, enrichment of heavy REEs and, sometimes, also the tetrad effect in their REE distribution patterns (Monecke et al., 2002), which is characteristic for the late Variscan Sn-W deposits. Samples from Dörfel and Ehrenfriedersdorf show both patterns (Fig. 5). Using linear discriminant analysis the samples can be classified by their relative content of light, medium, and heavy REEs (La, Gd, and Er; Fig. 6). This discrimination procedure yields high match for the polymetallic and Sn-W fluorites (89 and 97%, respectively). Consequently, the observed REE patterns of the selected samples correspond well to the two main mineralization periods.

(U-Th-Sm)/He ages

The summary of fluorite helium ages and the principal statistical data obtained on fluorites of the studied mining districts are compiled in Table 1, while the detailed raw data are listed in the electronic Appendix 2. The individual single fragment ages are plotted in Figure 7. Median FHe ages for the individual localities range from 79 to 234 Ma. Six out of seven localities yield Cretaceous median FHe ages between 79 and 112 Ma, only the Sadisdorf fluorite from the eastern Erzgebirge yields a Triassic median FHe age (Fig. 8). Except for this "oldest" sample the single-fragment aliquots yielded a reasonable confidence interval of the median (calculated by the method of Bonett and Price, 2002) below 11 Ma (Table 1).

Source of radiogenic helium

The ratio of the alpha-emitting, radioactive elements carry genetic information on fluorite formation and can be used as an index for the homogeneity of the studied fluorites. The U, Th, and Sm concentrations in the 233 dated single-fragment fluorite aliquots range between the level of detection and 35, 305, and 105 ppm, respectively. The average concentrations are ca. 0.8 ppm U, 12.5 ppm Th, and 12.3 ppm Sm. The contributions of the three alpha-emitting elements to the total radiogenic helium are highly variable (Fig. 9). It is possible to distinguish two types of localities. In case of the Zinnwald, Ehrenfriedersdorf, and Lauta samples, the sources of helium (from U, Th, or Sm) show characteristic proportions that define distinct compositional fields with only minor overlap (Fig. 9a). For instance, the He is derived mainly from Th in fluorites from Ehrenfriedersdorf, while in Lauta the Th contribution is subordinate. U-generated He is dominant in most Lauta samples while it is a minor component for the Zinnwald and Ehrenfriedersdorf sample. In some fluorites Sm-generated He is dominating, its contribution can be as high as 75% as, for example, in some Zinnwald samples. These relatively well-defined distributions indicate relative homogeneity of the fluorite crystals from these locations. In the other localities (Fig. 9b), the proportion of U-, Th-, and Sm-generated helium is not characteristic and the single-fragment aliquots show much wider scatter. These U-Th-Sm characteristics do not correlate to a late Variscan or Mesozoic formation age of the deposit. Thus, we assume that these features are principally controlled by the wave length and amplitude of the intracrystal zonation patterns and additional heterogeneities (as revealed by CL imaging) that are characteristic for a given sample and its formation history.

Discussion

Chemical heterogeneity and structural properties of the studied fluorites

Variations in chemical composition (e.g., REE distribution patterns, Y, U, and Th concentrations) reflect the formation conditions of hydrothermal fluorite influenced by the external supply of trace elements, remobilization of elements from the host rocks, fractionation of them in the hydrothermal environment, and during fluorite precipitation (Bau, 1991; Monecke et al., 2002, 2011; Schwinn and Markl, 2005). In this respect, there is a clear distinction between fluorites from Sn-W mineralization and samples from the Mesozoic polymetallic veins. Our data underline the contrasting chemical and structural characteristics of fluorite from the two mineralization types. For the Erzgebirge these differences are also constrained by chemical studies on fluid inclusions (Klemm, 1994) and Sr and Nd isotope investigations (Höhndorf et al., 1994).

There is not only a clear distinction between samples from the two mineralization types but also a variability in chemical composition and structure (expressed in color and in CL characteristics) within each mineralization group and at each locality (Figs. 5, 9, App. 2; cf. Kempe et al., 2002). For example, the high Th contents in the brownish fluorite sample (SD1001) from Sadisdorf and in the rose fluorite from an early cassiterite-bearing tourmaline veinlet at Ehrenfriedersdorf (ED 268) reflect the high Th activity at the early stages of evolution in tin-bearing hydrothermal systems (Morozov et al., 1996). The REE distribution pattern of the latter sample with depletion of light REEs (including Sm), enrichment of heavy REEs, and a small positive or no Eu anomaly is also typical of early fluorites

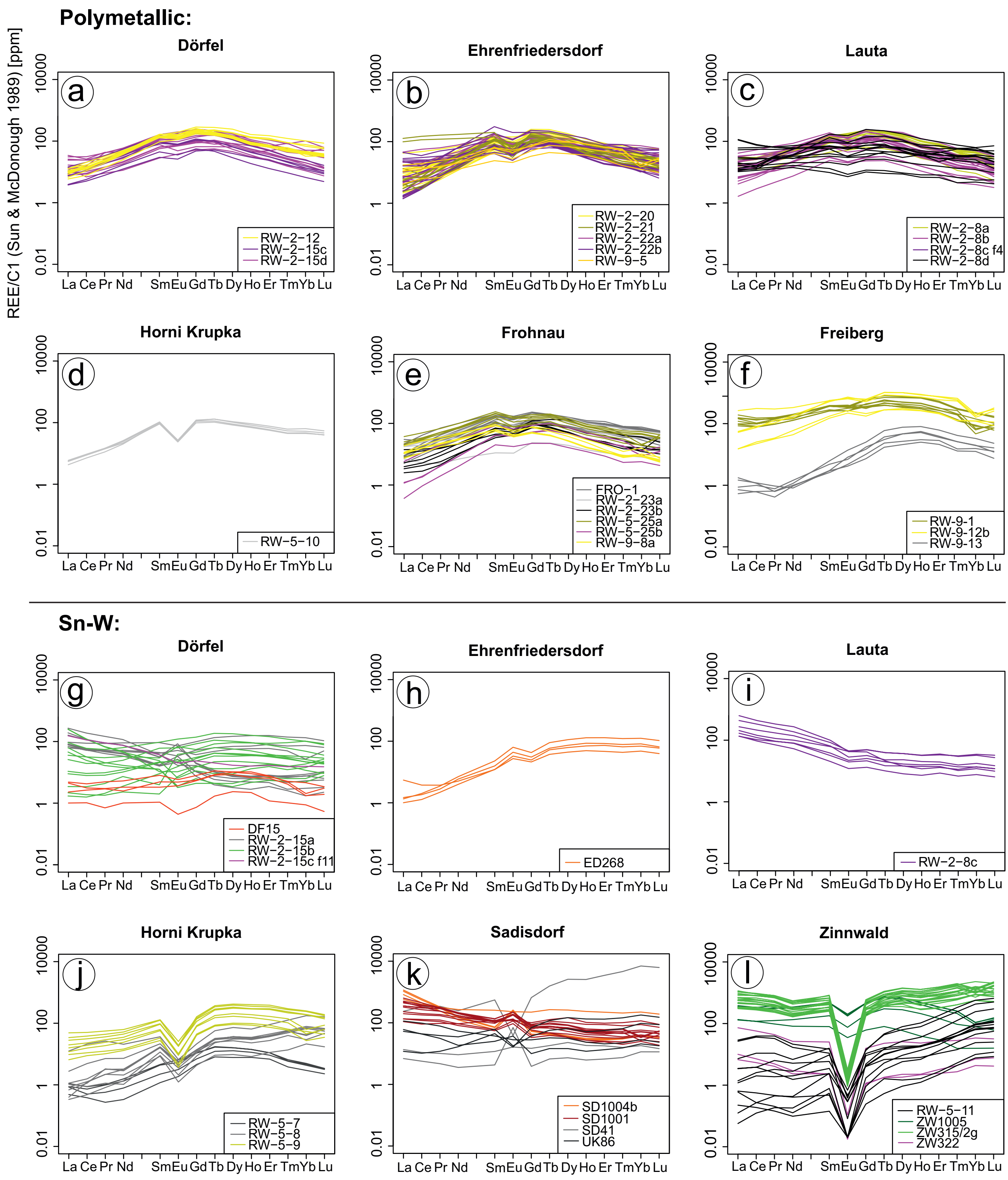

FIG. 5. REE distribution patterns of single crystal fragment fluorite samples (chondrite normalized after Sun and McDonough, 1989). The REE patterns illustrate the variability of chemical composition of fluorite studied. Fluorite from the Mesozoic polymetallic mineralization (a-f, hump-shaped patterns) and the late Variscan Sn-W deposits (g-l, Eu anomalies, heavy REE enrichment, and tetrad effect) can be distinguished clearly.

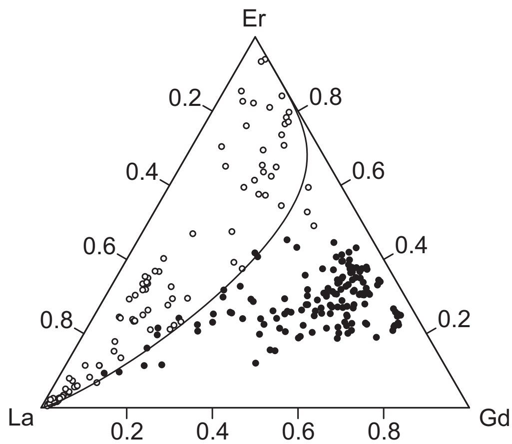

FIG. 6. Linear discrimination of polymetallic (black) and Sn-W (white) fluorite in ternary diagram using REE elements La, Gd, and Er.

from such deposits (Gavrilenko et al., 1997). Similarly, the high U content in fluorite from Lauta (Fig. 9) may be related to remobilization of U during vein formation, which is also mirrored by the occurrence of pitchblende in the paragenesis. Finally, there is an intrasample variability in composition and defect structure as demonstrated by CL imaging and spectroscopy (Fig. 4) but also by variations in chemical composition of single fragments derived from one individual crystal (Fig. 9). Structural variability and heterogeneity may influence FHe dating as will be discussed in more detail below.

Intrasample FHe age distributions

The number of aliquots analyzed from the mining localities ranges between 19 and 54, but typically exceeds 30 (Table 1); thus these data sets allow statistical treatment. Only some samples pass the chi-square normality test, while in case of the Lauta and Dörfel data the fitting to lognormal distribution is fair. In some other sample sets (e.g., Frohnau and Ehrenfriedersdorf) even a bimodal character with extremely old single-fragment aliquot ages from 250 to 300 Ma is possible (Fig. 7). Rejection of the few ages older than 200 Ma for Frohnau and Ehrenfriedersdorf let the remaining data sets pass the normality test.

The possible biasing factors that contribute to the considerable spread of single-fragment FHe ages are the following:

1. *Initial (nonradiogenic) helium:* During the formation of the fluorite crystals the ore-bearing fluids may carry a high amount of radiogenic noble gases (Ar and He). These gases may be trapped in fluid inclusions as "parentless" or "excess" helium (e.g., Fitzgerald et al., 2006). The only way to reduce their possible contribution is the careful selection of fluid inclusion-free aliquots. Working in alcohol immersion the achievable optical resolution is around 1 μm. As the selected crystal fragments did not contain any visible fluid inclusions the SEM investigations did not show submicrometer-sized inclusions. Thus we assume that the contribution of "parentless" He from fluids is negligible.

2. *Actinide- and Sm-rich refractory inclusions:* If refractory mineral inclusions carry alpha-emitting elements and these minerals are not dissolved by the routine fluorite digestion techniques then we have a deficit of mother elements and the calculated ages became biased toward older ages. We rarely observed tiny inclusions close to optical resolution of the research microscope, but their high actinide content could not be approved by in situ analytical tests (SEM, EMPA, and LA-ICP-MS). The majority of the aliquots did not contain any visible inclusions and did not yield increased amounts of helium at the sequential reheating. Consequently, although unlikely, this source of bias cannot be excluded completely.

3. *Zonation, heterogeneity:* The alpha particle, ejected during radioactive decay, has a stopping distance of 13 to 14 μm in the fluorite lattice. This implies that the concentration of alpha-emitting elements and the accumulation of helium are not necessarily consistent at microscale. The CL mappings indicate that fragments with a typical size of 100 to 400 μm, used for dating, may contain He or actinide anomalies. Therefore, the zoned character of the crystals definitely contributes to the scatter in the single-fragment ages. This is supported by the fact that the FHe ages of the samples having definite U/Th/Sm ratios (Fig. 9a) yield lower relative standard deviations of the single-fragment age distributions than the samples with highly variable U/Th/Sm ratios (Fig. 9b)—38 and 50%, respectively.

4. *Variation in He diffusivity:* From former studies (Evans et al., 2005; Pi et al., 2005) and own preliminary laboratory experiments it appears that the closure temperature of fluorite is highly variable. We assume that the observed variability in chemical composition and defect structures and densities causes significant intracrystal variation of diffusivity. If so, different domains in a given fluorite crystal may have different closure temperatures and single-fragment ages are thus influenced by variable helium loss, resulting in the large age scatter observed in the data. This point is of principle importance for FHe thermochronology and will be discussed in more detail in a forthcoming paper.

5. *Analytical uncertainty:* The precision of He, U, Th, and Sm measurements can be estimated by repeated measurement of certified reference materials. In case of our fluorite fragments, the amounts of actinides and Sm are considerably less compared to the routinely dated apatite and zircon crystals. The masses of these elements were typically below 1 ng, often close to the detection limit as mirrored by the high relative standard error values (App. 2). This is a consequence of the single-fragment approach. By increasing the dated mass of fluorites by multifragment technique, the analytical uncertainty would be probably reduced.

From the biasing factors listed above, only the analytical uncertainty can be estimated numerically. A quantitative estimation of the contributions from the other four factors is not feasible. Due to the typically asymmetric character of the single-aliquot FHe age distributions we prefer to express the averages by using locality medians as detailed in the following discussion. The right-hand asymmetry of the distributions has no diagnostic meaning in this approach. The He and radioactive element measurements have assumable Gaussian error distributions; their division (alike the age equation) results in a lognormal-like distribution with the long tail toward older ages. The other biasing factors (1) to (5) are usually also positively skewed and they are superimposed on the analytical uncertainty resulting in the total errors.

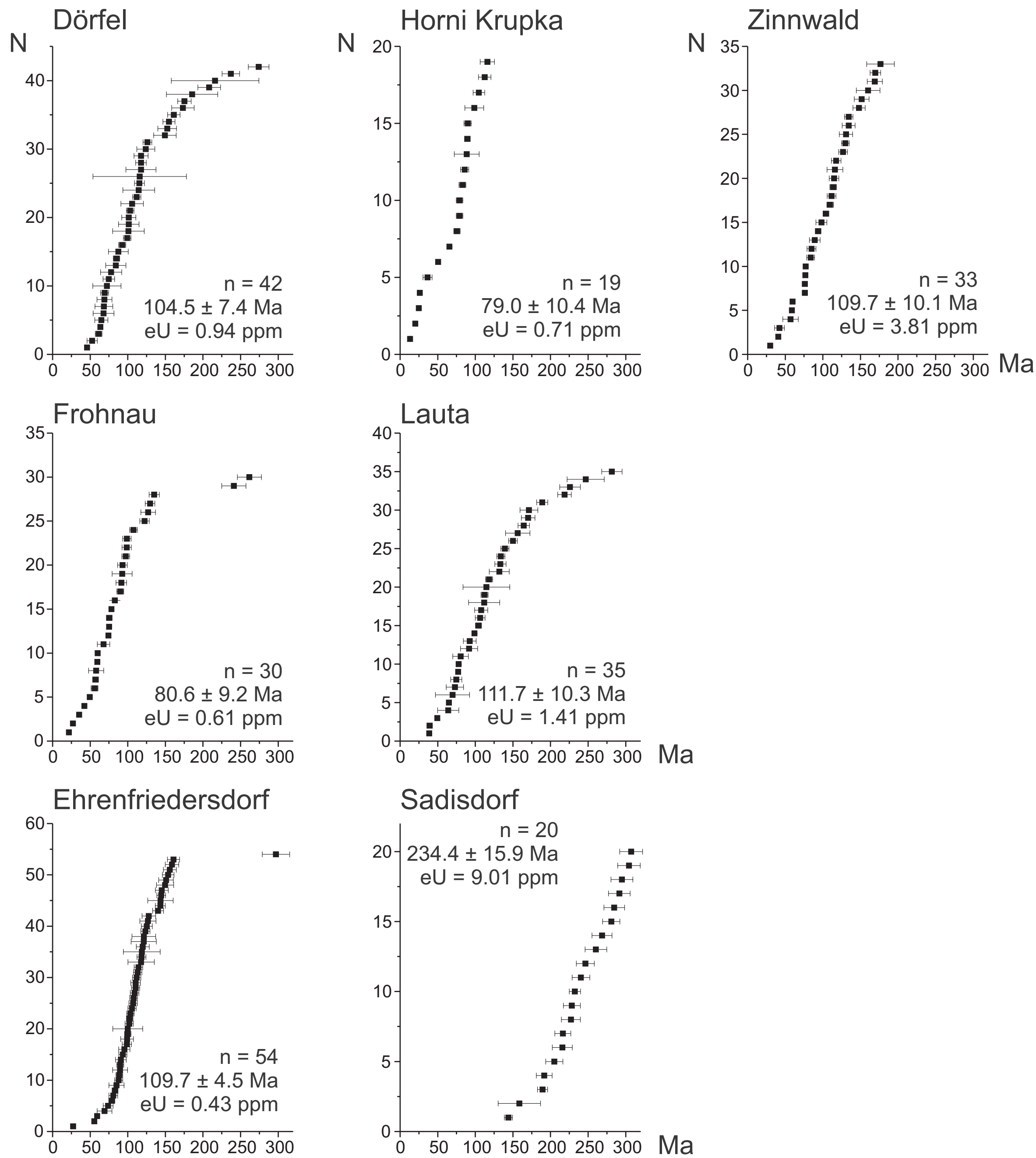

FIG. 7. Increasing scatter plot of the single-fragment fluorite (U-Th-Sm)/He ages. eU values (effective uranium concentration, a parameter that weights the decay of the two parents for their alpha productivity, computed as [U]ppm + 0.235 * [Th] ppm) vary between 0.43 and 9.01 ppm. The ages refer to the median and its respective confidence interval for each locality (Table 1).

Geological meaning of fluorite (U-Th-Sm)/He ages

In general, low-temperature thermochronology-like fission track and (U-Th-Sm)/He methods yield ages that can be classified into three categories following the approach of Wagner (1972):

1. If the mineral experienced rapid cooling immediately after its formation, then the undisturbed thermochronometer accumulates the products of radioactive decay and the measured age expresses a formation age. This scenario is typical for volcanic rocks. However, low-temperature thermochronology of hydrothermal mineralization may also yield formation ages when the orebody experienced rapid cooling and was not influenced by a later thermal overprint.

2. If the mineral experienced longlasting cooling after formation (or after a high-T event that caused complete reset), then the radioactive decay products disappear from the mineral until the system finally cools below the closure temperature of the given thermochronometer. Such cooling ages are typical for metamorphic units and the age provides a datum

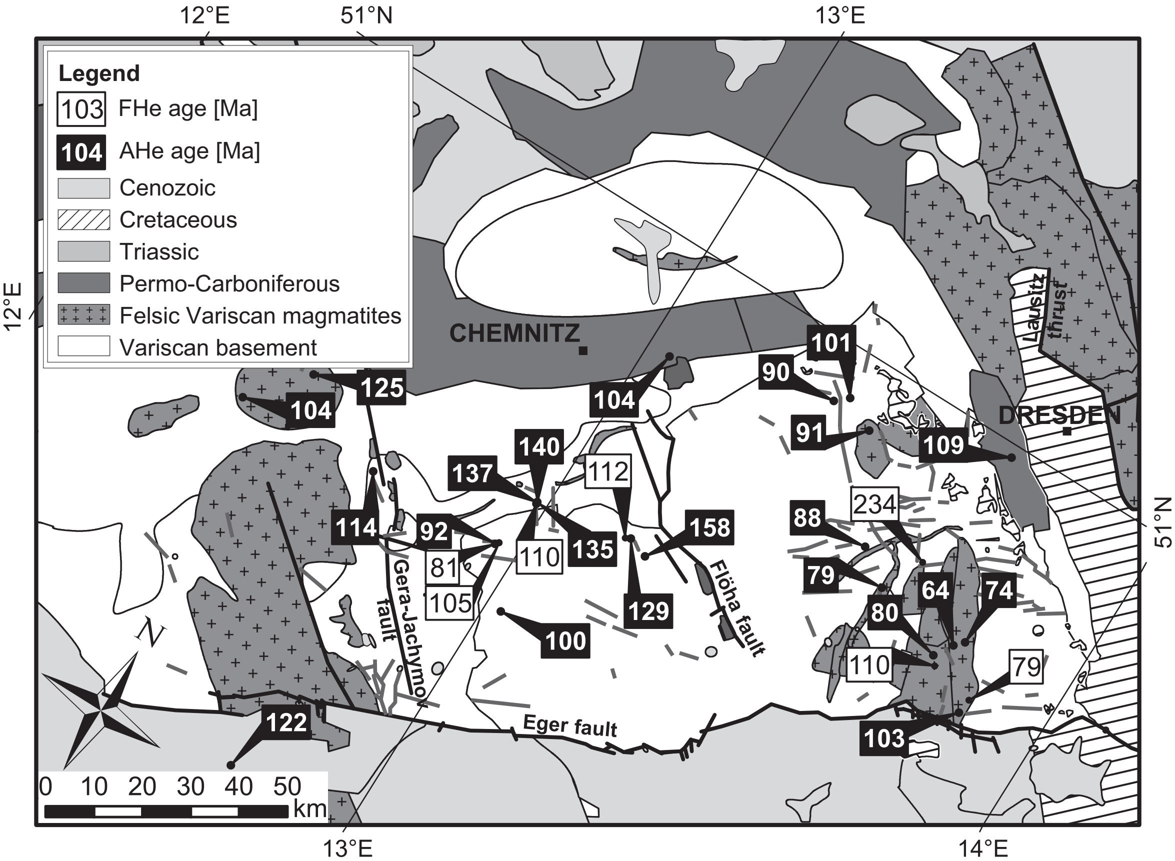

FIG. 8. Simplified geologic map of the Erzgebirge with median fluorite (U-Th-Sm)/He ages (black numbers; this study) and apatite (U-Th-Sm)/He ages (white numbers; Wolff et al., 2015). The ages are given in Ma, uncertainties and further analytical details are listed in the Appendix 1.

when the sample passed the temperature range of the so-called partial annealing zone (nuclear tracks) or partial retention zone (He thermochronology).

3. Complex thermal histories result in mixed ages when one or more thermal events cause only partial loss of decay products. This is characteristic for slightly (re-)heated formations, for instance, shallow burial in sedimentary basins or host bodies of hydrothermal deposits, when the temperature and the effective heating time of the hydrothermal activity were not sufficient for total reset. In this case, measured ages are younger than the formation age, but they do not express the age of any particular distinct cooling event.

Despite the high variability in mineral paragenesis, chemical composition, real structure, internal textures, and formation age of the fluorite samples, there is an overall consistence in the single-fragment age distributions for six of the seven studied localities. The first step in the evaluation of our FHe ages is the comparison of the low-temperature age constraints to the known formation ages. In case of fluorites from Sn-W mineralizations, the formation ages are certainly late Variscan, ca. 325 or 300 Ma, according to Romer et al. (2007, 2010a) or Kempe et al. (2004), respectively. The locality medians of the FHe ages, however, are mainly Cretaceous (112–79 Ma). Only the Sadisdorf site yields an older Triassic age (234 Ma), but this age is also significantly younger than Variscan. Therefore, an interpretation of the FHe ages from the late Variscan Sn-W deposits as formation ages must be rejected.

In case of fluorites from the younger, polymetallic mineralizations the situation is less clear because there are no paragenetic or textural evidences on their formation ages. Furthermore, the isotope geochronometers used in former studies indicate a wide spread of (frequently mixed) ages (see Fig. 2a). Thus, the formation age of the veins is hardly known. The fluid inclusion data indicate that the minimum formation temperature of fluorite in Mesozoic mineralizations of the central Erzgebirge, including Lauta and Ehrenfriedersdorf, was in the range between 200° and 320°C (Jung and Meyer, 1991; Klemm, 1994; Seifert et al., 1994). This temperature range can perform nearly complete He reset in probably already-existing fluorite crystals when the duration of effective heating time of the hydrothermal activity exceeds ca. 500 years (estimated according to Arehart et al., 2003). This is a conservative estimate for the time span of the activity of a fluid mobilization system (e.g., Goldfarb et al., 1991; Yardley and Cleverley, 2013). This implies that the FHe ages determined that polymetallic deposits should be interpreted as cooling ages.

The interpretation of the median FHe ages from six localities as Cretaceous cooling ages is further supported by some recent literature data from the region. Siebel et al. (2010) studied the thermal history in the intracontinental Danube

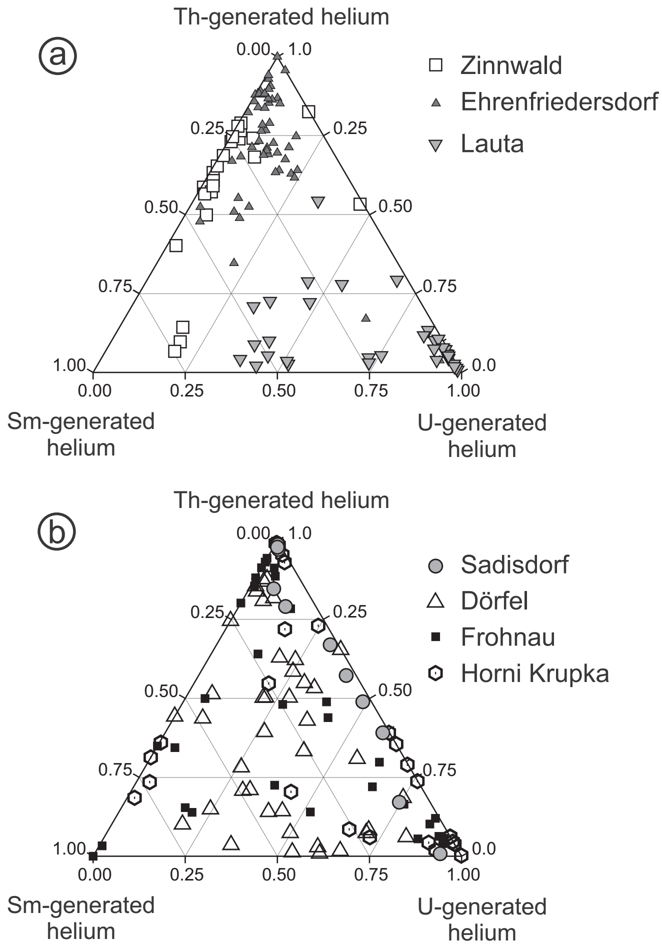

FIG. 9. The contributions of the three alpha-emitting elements to the total radiogenic helium budget of the dated fluorite samples. In three samples, the radioactive element ratios are roughly diagnostic (a), while in the other four samples the ratios are highly variable and do not discriminate the samples (b).

fault zone near Regensburg, Germany, located to the southwest of the Erzgebirge, by a multichronology approach. Few FHe ages obtained from fluorite samples of the Kittenrain fluorite vein deposit spread around 130 to 110 Ma and were interpreted as a result of partial reset of the isotope system during reactivation of the Danubian fault during the Cretaceous, while the fluorite mineralization is interpreted to be late Variscan in accordance with the late Variscan age of the primary pitchblende formation in the region. We note here the analogy to the late Variscan age and remobilization of U mineralization in the Erzgebirge region.

CL imaging reveals alteration textures in the fluorite crystals, which points to secondary processes at elevated temperatures. If the latest, fluorite-generating hydrothermal phase is close to the time of the thermal climax of the main mineralization period then the FHe age practically reflects the age of the ore-forming process. Recently, Ostendorf et al. (2014) performed direct age determination on the Mesozoic polymetallic or fluorite-barite mineralization at Freiberg, Germany, using the Rb-Sr isochron method on sphalerite. The reported age of 113 ± 4 Ma is in accordance with or slightly predates our Cretaceous FHe ages on the Mesozoic mineralization elsewhere in the Erzgebirge region (Table 1). Thus, the interpretation of Cretaceous FHe ages as formation ages cannot be rejected completely. Moreover, the FHe ages suggest that the Mesozoic thermal event terminated before latest Cretaceous, i.e., at around 80 Ma. Whether this thermal event is caused by hydrothermal activity has to remain unsettled in this case. A later Tertiary overprint is not recognized by the FHe method. This result is consistent with observations from apatite (U-Th)/He data (Wolff et al., 2015).

The four Sadisdorf fluorite samples gave consistent and considerably older (U-Th-Sm)/He ages than those from the other mining districts (Table 1). The Triassic FHe age can be interpreted in two ways. The first option is that this deposit experienced shallow post-Variscan burial and was only weakly affected by the Mesozoic thermal events. Thus it experienced minor rejuvenation from the original late Variscan age due to the weaker Mesozoic overprint. Alternatively, we can assume that the overprint is uniform in the region, but this fluorite has anomalous helium diffusivity behavior with higher closure temperature resulting in only minor helium loss during the Mesozoic thermal event. In any case, as we cannot assign a well-defined Triassic tectono-thermal event to this site—this age is interpreted as a mixed age.

The oldest single-fragment ages of the likely bimodal data sets from Frohnau and Ehrenfriedersdorf (three fragments with FHe ages between 241 and 297 Ma; see Fig. 8 and App. 2) raise the question whether the fluorites of the tin and polymetallic ore deposits have kept some memory of their formation in the late Variscan. This would be possible when low He diffusivity in some crystal domains have kept the old age information despite of some Mesozoic thermal overprint. These old FHe ages are in accordance with the formation age of the Sn-W mineralization in the western Erzgebirge constrained earlier by the zircon U-Pb method (Kempe et al., 2004). Such interpretation of the few older ages would also support a formation of at least a part of the polymetallic ore mineralization already in the late Variscan, probably shortly after the Sn-W deposits.

Relationships to other, well-established thermochronometers

The range of the defined median FHe ages corresponds well with the apatite (U-Th-Sm)/He (AHe) ages from the same ore districts (Figs. 2b, c, 8; Wolff et al., 2015). In the central block of the Erzgebirge, between the Gera-Jachymov and Flöha faults, as well as in the Zinnwald district, the apparent FHe ages and the apparent AHe ages are largely similar. Only the FHe ages from Sadisdorf samples are significantly older than the corresponding AHe ages (see discussion above). However, the AHe ages show a heterogeneous distribution in the study area (Fig. 8; Wolff et al., 2015). The data has been interpreted to reflect three major tectonic blocks with different thermal histories. Following the exhumation to a near-surface position after the Variscan orogeny the Erzgebirge basement suffered a Permo-Mesozoic burial temperature reaching ca. 80° to 100°C, while the sedimentary cover thins out toward north. The tectonic blocks are locally superposed by hydrothermal activity along well-defined pathways corresponding to the known vein deposits (Wolff et al., 2015). This pattern suggests a localized character of thermal anomalies that preferentially culminates in the ore districts. The resulting time-temperature conditions have caused a total reset of large parts of fluorite in most of the fluorite-bearing ore districts but possibly only a partial reset of the fluorite sample from the Sadisdorf deposit. Likely, the Erzgebirge did not suffer a single overall penetrative heating event.

The closure temperature of the FHe system was estimated at 170° and 60°C (Evans et al., 2005; Pi et al., 2005). Ongoing experiments point to the lower end of this closure temperature range for the fluorites analyzed herein. Even though these closure temperatures are still to be verified, it is noticeable that our new FHe age data not only overlap with the previously published AHe ages (Figs. 2c, 8) but also with the youngest hydrothermally reset zircon He ages in the Erzgebirge (ca. 134–112 Ma; Wolff et al., 2015). This as well suggests a closure temperature for the fluorite system just within the range reported, below the zircon He system (ca. 180°–160°C, Reiners et al., 2002) and similar to or slightly higher than the apatite system (ca. 80°–60°C, Farley, 2000).

Modeling of the thermal history by FHe age data

A measured FHe age, like any (U-Th-Sm)/He age, is the result of a thermal evolution path where the radiogenic helium production and the temperature-driven diffusional loss of helium (e.g., McDougall and Harrison, 1988). The concept of closure temperature (Dodson, 1973) describes the accumulation of daughter isotopes and the evolution of the age when the geologic formation is cooling monotonously. However, the description of complex thermal histories requires a more dynamic evaluation procedure that considers the known constraints of the regional thermal evolution and also the kinetic parameters of the dated mineral-method pair. Typically, apatite and zircon FT and (U-Th-Sm)/He thermochronological data supply the major input for the modeling of the low-temperature thermal history. In our study, the modeling is based, for the first time, on fluorite He ages and diffusion parameters.

For modeling of the thermal history, the HeFTy software (Ketcham, 2005) was used. Data from two characteristic mining sites from the central and eastern Erzgebirge were selected for this evaluation (Ehrenfriedersdorf and Zinnwald, respectively). Beyond FHe data, apatite fission track ages and track length distributions were available for Ehrenfriedersdorf, while for Zinnwald a wider temperature range was covered by zircon and apatite (U-Th-Sm)/He and apatite fission track data (samples A6 and D4, respectively; see Wolff et al., 2015). The helium diffusion parameters for fluorite have been estimated to be Ea = 33 kcal/mol and log D_0/a^2 = 4.0 s^{-1} according to our preliminary measurements. These values are in accordance with the published values of Ea = 30.5 kcal/mol and log D0/a2 = 4.9 s^{-1} (Evans et al., 2005). The resulting time-temperature paths are covered by envelopes and presented in Figure 10.

Results indicate that the thermal histories calculated from the fluorite (U-Th-Sm)/He data (Fig. 10, top) are quite similar to those calculated using well-established apatite (+ zircon) data (Fig. 10, bottom). The apatite- and zircon-based modeling yields a slightly narrower range of acceptable

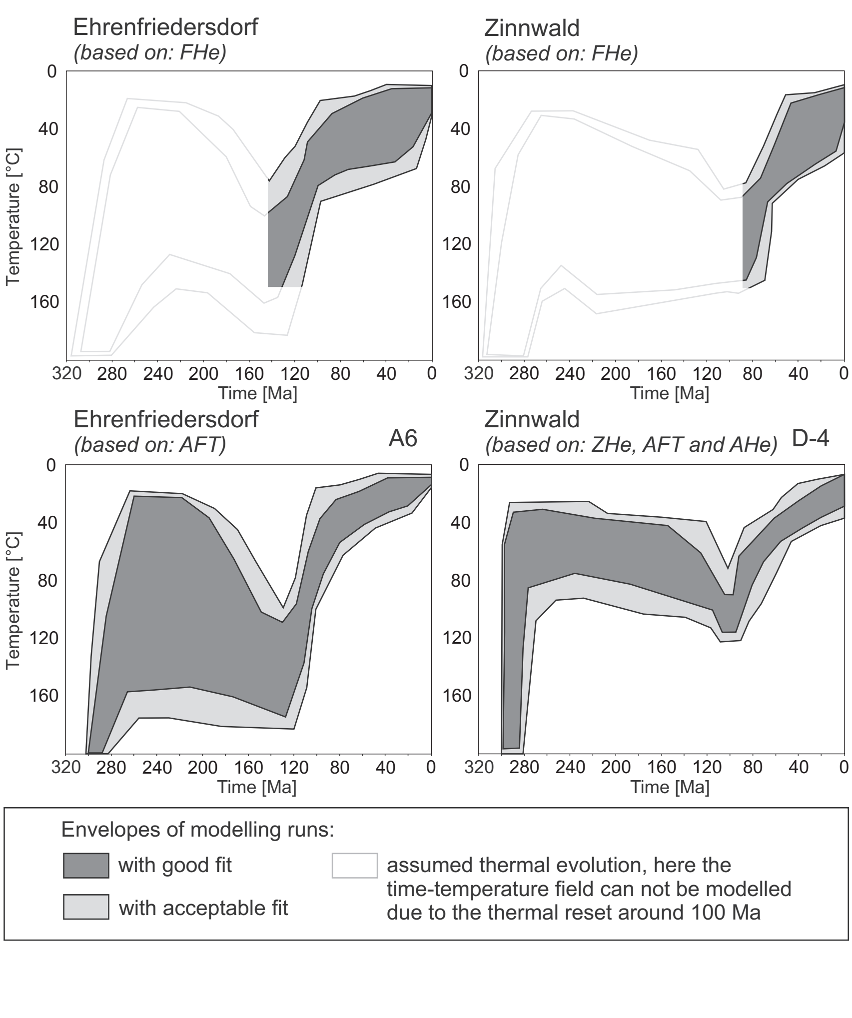

FIG. 10. Comparison of modeled thermal history based on the classic, widely used low-temperature thermochronometers (lower panels; Wolff et al., 2015) and the new, fluorite (U-Th-Sm)/He-based modeling results (upper panels). For modeling, the HeFTy software (Ketcham, 2005) was used; the applied diffusion parameters are explained in the text. The constraints of the modeling were identical for apatite and zircon and for the fluorite-based modeling runs. Envelopes of the acceptable time-temperature paths (corresponding to "goodness of fit" >0.05) shown by light gray fields and the envelopes of the "good fits" (GOF >0.5) by dark gray fields. The pre-Cretaceous thermal history cannot be properly constrained by FHe chronometer.

time-temperature envelopes compared to solely FHe-based modeling. This is to be expected and relates to the fact that the AFT data are associated with track length measurements that supply more parameters to constrain the thermochronological modeling. We conclude that thermal modeling of the fluorite (U-Th-Sm)/He data using HeFTy software and diffusion parameters determined on the dated fluorite crystals reveals geologically meaningful thermal histories that are largely similar to those derived by other thermochronological data.

Methodological outlook

In order to evaluate the applicability of the FHe method, a conservative approach has been chosen by analyzing single-fragment aliquots. In this way, we aimed to detect the limits of the applicability of the method. Our approach allows an evaluation of the effects of zonation and sample heterogeneity. The analysis of multifragment aliquots would be a more steady and pragmatic approach for further studies. This has been simulated by an n-fold validation, randomly creating multifragment aliquots from the single-fragment data. Using five-fragment aliquots the standard errors calculated for the localities are reduced significantly from the range of 16 to 5 Ma to a range between 2.9 and 0.8 Ma (see comparison in Table 2). These much narrower confidence intervals are largely similar to the typical error range of other low-temperature geochronological methods, and the multifragment technique would make fluorite (U-Th-Sm)/He thermochronology suitable for routine applications. On the other hand, the chemical variability as an indicator of the heterogeneity and zonation of the dated minerals gained by the single-fragments analyses is lost using the multifragment aliquot technique.

Conclusions

1. The fluorite (U-Th-Sm)/He method is well suited for ore deposits and hydrothermally altered regions where the well-established apatite-based low-temperature thermochronometers cannot be applied due to the high solubility of apatite in acid environments.
2. Modeling of FHe thermochronological data using diffusion parameters determined on the dated fluorite samples yields geologically meaningful thermal histories similar to results based on other well-established thermochronological methods.
3. The closure temperature range (or partial retention zone) of the FHe thermochronometer of chemically nonextreme fluorite (i.e., REE + Y <3,000 ppm) appears to be similar or somewhat higher compared to the He closure temperature in apatite and lower than the (U-Th-Sm)/He closure temperature in zircon. However, further studies on the diffusion behavior of He in fluorite are needed.
4. FHe data from six mining districts of the Erzgebirge indicate that the thermal activity in the studied area terminated before latest Cretaceous. A later, Tertiary thermal overprint is not recognized.
5. The Cretaceous thermal event was not able to reset the FHe thermochronometer all over the entire Erzgebirge as indicated by mixed ages for the Sadisdorf tin deposit.
6. The oldest FHe ages measured in a few aliquots might indicate that some polymetallic vein deposits in the Erzgebirge were generated already in the late Variscan.

Acknowledgments

This study was funded by the German Research Foundation (DFG grant DU373/6). We gratefully acknowledge the donation of mineral species by the mineral collection of the Technical University Bergakademie Freiberg and the Mining Museum of Altenberg. We are indebted to Irina Ottenbacher and Judit Dunkl-Nagy for the careful mineral separation and for the He measurements, and to the Central Metal Workshop of the Geoscience Center Göttingen for maintenance of the GÖochronology Laboratory. We further thank Raimon Tolosana-Delgado for his valuable support in discrimination analysis and R. Romer for critical comments on an earlier version of the manuscript. The reviewers Wolfgang Siebel and Ferenc Molnár greatly helped to improve the paper.

REFERENCES

Arehart, G.B., Chakurian, A.M., Tretbar, D.R., Christensen, J.N., McInnes, B.A., and Donelick, R.A., 2003, Evaluation of radioisotope dating of Carlin-type deposits in the Great Basin, western North America, and implications for deposit genesis: Economic Geology, v. 98, p. 235–248.

TABLE 2. Simulated n-Fold Validation, Randomly Creating Multifragment Aliquots from the Single-Fragment Data

	A. Dörfl (Ma)	s.d. (Ma)	A. Frohnau (Ma)	s.d. (Ma)	Efd. (Ma)	s.d. (Ma)	Horni Krupka (Ma)	s.d. (Ma)	Lauta (Ma)	s.d. (Ma)	Zinnwald (Ma)	s.d. (Ma)	Sadisdorf (Ma)	s.d. (Ma)
1st random selection	114	1.2	78	1.3	105	1.2	68	1.7	127	1.2	107	1.3	241	1.1
2nd repetition	115	1.2	89	1.2	111	1.1	79	1.4	126	1.3	112	1.2	241	1.1
3rd repetition	117	1.3	86	1.4	112	1.2	73	1.2	111	1.3	100	1.1	248	1.1
4th repetition	117	1.2	80	1.3	106	1.3	76	1.3	127	1.3	103	1.1	239	1.0
5th repetition	117	1.2	81	1.4	106	1.2	73	1.2	127	1.2	103	1.2	232	1.2
6th repetition	112	1.3	96	1.3	108	1.1	70	1.1	115	1.2	107	1.2	249	1.1
Descriptive statistics of multifragment aliquot ages														
mean	115.3		85.0		108.0		73.2		122.2		105.3		241.7	
s.d.	2.1		6.8		2.9		4.0		7.2		4.2		6.3	
s.e.	0.8		2.8		1.2		1.6		2.9		1.7		2.6	
Descriptive statistics of single-fragment aliquot ages														
mean	116.6		90.2		113.1		70.5		122.3		104.9		239.4	
s.e.	8.1		9.6		5.1		7.4		9.9		6.8		10.6	

Abbreviations: s.d. = standard deviation, s.e. = standard error

Bau, M., 1991, Rare-earth element mobility during hydrothermal and metamorphic fluid-rock interaction and the significance of the oxidation state of europium: Chemical Geology, v. 93, p. 219–230.

Baumann, L., 1967, Zur Frage der varistischen und postvaristischen Mineralisation im sächsischen Erzgebirge: Freiberger Forschungshefte C, v. 209, p. 15–38.

——1994a, Ore parageneses of the Erzgebirge—history, results and problems: Monograph Series, Mineral Deposits, v. 31, p. 25–46.

——1994b, The vein deposits of Freiberg, Saxony: Monograph Series, Mineral Deposits, v. 31, p. 149–167.

Baumann, L., and Weber, W., 1996, Crust activation in central Europe and their metallogenetic importance for the Erzgebirge: Freiberger Forschungshefte C, v. 467, p. 27–58.

Baumann, L., Kuschka, E., and Seifert, T., 2000, Lagerstätten des Erzgebirges: Stuttgart, Enke im Thieme Verlag, 300 p.

Bonett, D.G., and Price, R.M., 2002, Statistical inference for a linear function of medians: Confidence intervals, hypothesis testing and sample size requirements: Psychological Methods, v. 7, p. 370–383.

Brause, H., 1988, Beiträge zur Geodynamik des Saxothuringikums: Geoprofil, v. 2, p. 1–88.

Cathelineau, M., Boiron, M., Holliger, P., and Poty, B., 1990, Metallogenesis of the French part of the Variscan orogen. Part II: Time-space relationships between U, Au and Sn-W ore deposition and geodynamic events—mineralogical and U-Pb data: International IGCP Conference Project 233: Tectonophysics, v. 177, p. 59–79.

Chesley, J.T., Halliday, A.N., and Scrivener, R.C., 1991, Samarium-neodymium direct dating of fluorite mineralization: Science, v. 252, p. 949–951.

Chesley, J., Halliday, A.N., Kyser, T.K., and Spry, P.G., 1994, Direct dating of Mississippi Valley-type mineralization: Use of Sm-Nd in fluorite: Economic Geology, v. 89, p. 1192–1199.

Danišík, M., Migoń, P., Kuhlemann, J., Evans, N.J., Dunkl, I., and Frisch, W., 2010, Thermochronological constraints on the long-term erosional history of the Karkonosze Mts., Central Europe: Geomorphology, v. 117, p. 78–89.

Dodson, M.H., 1973, Closure temperature in cooling geochronological and petrological systems: Contributions to Mineralogy and Petrology, v. 40, p. 259–274.

Dolejs, D., and Štemprok, M., 2001, Magmatic and hydrothermal evolution of Li-F granites: Cinovec and Krasno intrusions, Krusne hory batholith: Czech Republic Bulletin of Geoscience, v. 76, p. 77–99.

Dudek, A., Frolíková, I., and Nekovarík, Č., 1991, The depth of intrusion of Hercynian granitoid plutons in the Bohemian massif: Acta Universitatis Carolinae Geologica, v. 3, p. 1–4.

Eikenberg, J., 1991, Application of the U-Xe-Kr and U-Pb systems for dating U-minerals, *in* Pagel, M., and Leroy, L., eds., Source, transport and deposition of metals: Rotterdam, Balkema, p. 385–390.

Eissmann, L., 1997, Die ältesten Berge Sachsens oder die morphologische Beharrlichkeit geologischer Strukturen, mit 2 Tabellen: Altenburger naturwissenschaftliche Forschungen: Altenburg, Naturkundliches Museum, 56 p.

Evans, N.J., Wilson, N., Cline, J., McInnes, B.I.A., and Byrne, J., 2005, Fluorite (U-Th)/He thermochronology: Constraints on the low temperature history of Yucca Mountain, Nevada: Applied Geochemistry, v. 20, p. 1099–1105.

Farley, K.A., 2000, Helium diffusion from apatite: General behavior as illustrated by Durango fluorapatite: Journal of Geophysical Research, v. 105, p. 2903–2914.

Farley, K.A., Wolf, R.A., and Silver, L., 1996, The effects of long alpha-stopping distances on (U-Th)/He ages: Geochimica et Cosmochimica Acta, v. 60, p. 4223–4229.

Fitzgerald, P.G., Baldwin, S.L., Webb, L.E., and O'Sullivan, P.B., 2006, Interpretation of (U-Th)/He single grain ages from slowly cooled crustal terranes: A case study from the Transantarctic Mountains of southern Victoria Land: Chemical Geology, v. 225, p. 91–120.

Förster, B., and Haack, U., 1996, Multistage evolution of the Aue-Niederschlema uranium vein deposit (Erzgebirge, Germany): Evidence from pitchblende dating [abs.]: Journal of Conference Abstracts, v. 1, p. 173.

Gavrilenko, V., Morozov, M., Kempe, U., Smolenskiy, V., and Wolf, D., 1997, Unusual REE distribution patterns in fluorites from Sn-W deposits of the quartz-cassiterite and quartz-wolframite type [abs.]: Journal of Czech Geological Society, v. 42, p. 36.

Goldfarb, R.J., Snee, L.W., and Miller, L.D., 1991, Rapid dewatering of the crust deduced from ages of mesothermal gold deposits: Nature, v. 354, p. 296–298.

Götze, J., 1998, Geochemistry and provenance of the Altendorf feldspathic sandstone in the Middle Bunter of the Thuringian basin (Germany): Chemical Geology, v. 150, p. 43–61.

Grønlie, A., Harder, V.M., and Roberts, D., 1990, Preliminary fission-track ages of fluorite mineralisation along fracture zones, inner Trondheimsfjord, Central Norway: Norsk Geologisk Tidsskrift, v. 70, p. 173–178.

Halliday, A.N., and Mitchell, J.G., 1984, K-Ar ages of clay-size concentrates from the mineralisation of the Pedroches batholith, Spain, and evidence for Mesozoic hydrothermal activity associated with the break up of Pangaea: Earth and Planetary Science Letters, v. 68, p. 229–239.

Hofstra, A.H., Premo, W.R., Emsbo, P., Cline, J.S., and Aleinikoff, J.N., 2000, U-Th-Pb dating of hydrothermal minerals from Carlin-type gold deposits: Results and evaluation, *in* Cluer, J.K., Price, J.G., Struhsacker, E.M., Hardyman, R.F., and Morris, C.L., eds, Geology and Ore Deposits 2000: The Great Basin and Beyond, Geological Society of Nevada Symposium Proceedings, Reno, Nevada, p. 61–65.

Höhndorf, A., Kämpf, H., and Dulski, P., 1994, Sm/Nd and Rb/Sr isotopic investigations on fluorite mineralization of the eastern Erzgebirge, *in* Seltmann, R., Kämpf, H., and Möller, P., eds., Metallogeny of collisional orogens focussed on the Erzgebirge and comparable metallogenic settings: Prague, Czech Republic, Czech Geological Survey, p. 116–128.

Hösel, G., Meyer, H., and Tägl, U., 1994, Sauberg/Westfeld, *in* Hösel, G., ed., Das Zinnerz-Lagerstättengebiet Ehrenfriedersdorf/Erzgebirge: Freiberg, Bergbau in Sachsen, Landesamt für Umwelt und Geologie und Oberbergamt, v. 1, p 42–58.

Janetschke, N., and Wilmsen, M., 2014, Sequence stratigraphy of the lower Upper Cretaceous Elbtal Group (Cenomanian-Turonian of Saxony, Germany): Zeitschrift der Deutschen Gesellschaft für Geowissenschaften, v. 165, p. 179–207.

Jung, D., and Meyer, H., 1991, Zur Geologie der Lagerstätte Röhrenbohrer: Geoprofil, v. 3, p. 21–27.

Kempe, U., and Götze, J., 2002, Cathodoluminescence (CL) behaviour and crystal chemistry of apatite from rare-metal deposits: Mineralogical Magazine, v. 66, p. 151–172.

Kempe, U., Plötze, M., Brachmann, A., and Böttcher, R., 2002, Stabilisation of divalent rare earth elements in natural fluorite: Mineralogy and Petrology, v. 76, p. 213–234.

Kempe, U., Bombach, K., Matukov, D., Schlothauer, T., Hutschenreuter, J., Wolf, D., and Sergeev, S., 2004, Pb/Pb and U/Pb zircon dating of subvolcanic rhyolite as a time marker for Hercynian granite magmatism and Sn mineralisation in the Eibenstock granite, Erzgebirge, Germany: Considering effects of zircon alteration: Mineralium Deposita, v. 39, p. 646–669.

Ketcham, R.A., 2005, Forward and inverse modeling of low-temperature thermochronometry data: Reviews in Mineralogy and Geochemistry, v. 58, p 275–314.

Klemm, W., 1994, Review of data on the composition of hydrothermal solutions during the Variscan and post Variscan mineralizations in the Erzgebirge, Germany: Monograph Series, Mineral Deposits, v. 31, p. 61–69.

Kley, J., 2013, Saxonian tectonics in the 21st century: Zeitschrift der Deutschen Gesellschaft für Geowissenschaften, v. 164, p. 295–311.

Knobloch, E., Konzalová, M., and Kvacek, Z., 1996, Die obereozäne Flora der Staré Sedlo-Schichtenfolge in Böhmen (Mitteleuropa): Rozpravy Česke Geologicke Ustavu Svazek, v. 49, p. 1–260.

Kossmat, F., 1925, Übersicht der Geologie von Sachsen: Erläuterung zu den vom Sächsischen Geologischen Landesamt veröffentlichten Übersichtskarten, 2nd, Leipzig, Hauptvertriebshandlung, Dresden, G.A. Kaufmanns Buchhandlung.

Kroner, U., Hahn, T., Romer, R.L., and Linnemann, U., 2007, The Variscan orogeny in the Saxo-Thuringian zone-heterogeneous overprint of Cadomian/Palaeozoic peri-Gondwana crust: Geological Society of America Special Paper 423, p. 153–172.

Kumann, R., and Leeder, O., 1994, On the relations between granite and ore in the Ehrenfriedersdorf tin deposit, Erzgebirge, *in* Seltmann, R., Kämpf, H., and Möller, P., eds., Metallogeny of collisional orogens focussed on the Erzgebirge and comparable metallogenic settings: Prague, Czech Republic, Czech Geological Survey, p. 166–173.

Kuschka, E., 1996, Hydrothermalite des Schwarzwaldes und Erzgebirges im paragenetischen Vergleich: Freiberger Forschungshefte C, v. 467, p. 177–200.

——1997, Atlas der hydrothermalite des Vogtlandes, Erzgebirges und Granulitgebirges. Sächsisches Landesamt für Umwelt und Geologie, Bereich Boden und Geologie: Geoprofil, v. 10, p. 1–151.

Lange, J., Tonk, C., and Wagner, G.A., 2008, Apatite fission track data for the Postvariscan thermotectonic evolution of the Saxon basement: First results: Zeitschrift der Deutschen Gesellschaft für Geowissenschaften, v. 159, p. 123–132.

Linnemann, U., and Romer, R.L., 2002, The Cadomian orogeny in Saxo-Thuringia, Germany: Geochemical and Nd-Sr-Pb isotopic characterization of marginal basins with constraints to geotectonic setting and provenance: Massifs and correlations across the Cadomo-Avalonian orogens: Tectonophysics, v. 352, p. 33–64.

——2010, Pre-Mesozoic geology of Saxo-Thuringia: From the Cadomian active margin to the Variscan orogen: Stuttgart, Schweizerbart, 485 p.

McDougall, I., and Harrison, T.M., 1988, Geochronology and thermochronology by the $^{40}Ar/^{39Ar}$ method: New York, Oxford University Press, xi, 212 p.

Mitchell, J.G., and Halliday, A.N., 1976, Extent of Triassic/Jurassic hydrothermal ore deposits on the North Atlantic margins: Transactions of the Institution of Mining and Metallurgy, sec. B, v. 85, p. 159–161.

Monecke, T., Kempe, U., Monecke, J., Sala, M., and Wolf, D., 2002, Tetrad effect in rare earth element distribution patterns: A method of quantification with application to rock and mineral samples from granite-related rare metal deposits: Geochimica et Cosmochimica Acta, v. 66, p. 1185–1196.

Monecke, T., Kempe, U., Trinkler, M., Thomas, R., Dulski, P., and Wagner, T., 2011, Unusual rare earth element fractionation in a tin-bearing magmatic-hydrothermal system: Geology, v. 39, p. 295–298.

Morozov, M., Trinkler, M., Plötze, M., and Kempe, U., 1996, Spectroscopic studies on fluorites from Li-F and alkaline granite systems in Central Kazakhstan, *in* Shatov, V., Seltmann, R., Kremenetsky, A., Lehmann, B., Popov, V., and Ermolov, P., eds., Granite-related ore deposits of Central Kazakhstan and adjacent areas: St. Petersburg, Project, p. 359–369.

Ostendorf, J., Henjes-Kunst, F., Seifert, T., and Gutzmer, J., 2014, Rb-Sr geochronology of sphalerite from fluorite-barite-sulfide veins of the Freiberg ore district, Erzgebirge (Germany) [abs.]: International Mineralogical Association (IMA) General Meeting 2014, 21st, Johannesburg, South Africa, Abstract ID: 664.

Pi, T., Solé, J., and Taran, Y., 2005, (U-Th)/He dating of fluorite: Application to the La Azul fluorspar deposit in the Taxco mining district, Mexico: Mineralium Deposita, v. 39, p. 976–982.

Pietzsch, K., 1913, Verwitterungserscheinungen der Auflagerungsfläche des sächsischen Cenomans: Zeitschrift der Deutschen Gesellschaft für Geowissenschaften, v. 65, p. 594–602.

Prazak, J., 1994, Cretaceous: Geological Atlas of the Czech Republic, Stratigraphy, 1st ed., Český geologický ústav, Kutná Hora.

Reiners, P.W., Farley, K.A., and Hickes, H., 2002, He diffusion and (U-Th)/He thermochronometry of zircon: Initial results from Fish Canyon Tuff and Gold Butte: Tectonophysics, v. 349, p. 297–308.

Romer, R.L., Thomas, R., Stein, H., Rhede, D., 2007, Dating multiply overprinted Sn-mineralized granites—examples from the Erzgebirge, Germany: Mineralium Deposita, v. 42, p. 337–359.

Romer, R.L., Förster, H., and Štemprok, M., 2010a, Age constraints for the late-Variscan magmatism in the Altenberg-Teplice caldera (Eastern Erzgebirge/Krušné hory): Neues Jahrbuch für Mineralogie Abhandlungen, v. 187, p. 289–305.

Romer, R.L., Schneider, J., and Linnemann, U., 2010b, Post-Variscan deformation and hydrothermal mineralization in Saxo-Thuringia and beyond: A review, *in* Linnemann, U., and Romer, R.L., eds., Pre-Mesozoic geology of Saxo-Thuringia. From the Cadomian active margin to the Variscan orogen: Stuttgart, Schweizerbart, p. 347–360.

Schröder, B., 1976, Saxonische Tektonik im Ostteil der Süddeutschen Scholle: International Journal of Earth Sciences (Geologische Rundschau), v. 65, p. 34–54.

——1987, Inversion tectonics along the western margin of the Bohemian massif: Compressional intra-plate deformations in the Alpine foreland: Tectonophysics, v. 137, p. 93–100.

Schröder, B., and Peterek, A., 2001, Cenozoic degradation history of basement units in the surroundings of the western Eger (Ohre) rift: Zeitschrift der Deutschen Gesellschaft für Geowissenschaften, v. 152, p. 387–403.

Schwinn, G., and Markl, G., 2005, REE systematics in hydrothermal fluorite: Chemical Geology, v. 216, p. 225–248.

Seifert, T., 2008, Metallogeny and petrogenesis of lampophyres in the Mid-European variscides: Post-collosional magmatism and its relationship to late-variscan ore forming processes in the Erzgebirge (Bohemian massiv): Rotterdam, IOS Press, 303 p.

Seifert, T., Baumann L., and Leeder O., 1992, Contribution to the paragenetic characterization of mineralizations of the Sn (-W), quartz-polymetal and fluorite-quartz association in the E part of the Central Erzgebirge anticlinal area: Neues Jahrbuch für Mineralogie Abhandlungen, v. 165, p. 65–81.

Seifert, T., Wendebaum, G., Trinkler, M., and Baumann, L., 1994, Geochemische und thermometrische Untersuchungen an hydrothermalen Mineralisationen im Mittleren Erzgebirge: European Journal of Mineralogy, v. 6, p. 261.

Siebel, W., Hann, H.P., Danišík, M., Shang, C.K., Berthold, C., Rohrmüller, J., Wemmer, K., and Evans, N.J., 2010, Age constraints on faulting and fault reactivation: A multi-chronological approach: International Journal of Earth Sciences (Geologische Rundschau), v. 99, p. 1187–1197.

Stemprok, M., and Sulcek, Z., 1969, Geochemical profile through an ore-bearing lithium granite: ECONOMIC GEOLOGY, v. 64, p. 392–404.

Suhr, P., 2003, The Bohemian massif as a catchment area for the NW European Tertiary basin: Geolines, v. 15, p. 147–159.

Sun, S., and McDonough, W.F., 1989, Chemical and isotopic systematics of oceanic basalts: Implications for mantle composition and processes: Geological Society, London, Special Publication 42, p. 313–345.

Thomson, S.N., and Zeh, A., 2000, Fission-track thermochronology of the Ruhla Crystalline Complex: New constraints on the post-Variscan thermal evolution of the NW Saxo-Bohemian Massif: Tectonophysics, v. 324, p. 17–35.

Tischendorf, G., 1989, Silicic magmatism and metallogenesis of the Erzgebirge [compiled]: Veröffentlichungen des Zentralinstitutes für Physik der Erde, v. 107, Potsdam, 316 p.

Tischendorf, G., and Förster, H., 1990, Acid magmatism and related metallogenesis in the Erzgebirge: Geological Journal, v. 25, p. 443–454.

Trinkler, M., Monecke, J., and Thomas, R., 2005, Constraints on the genesis of yellow fluorite in hydrothermal barite-fluorite veins of the Erzgebirge, eastern Germany: Evidence from optical absorption spectroscopy, rare-earth-element data, and fluid-inclusion investigations: Canadian Mineralogist, v. 43, p. 883–898.

Ventura, B., and Lisker, F., 2003, Long-term landscape evolution of the northeastern margin of the Bohemian massif: Apatite fission-track data from the Erzgebirge (Germany): International Journal of Earth Sciences (Geologische Rundschau), v. 92, p. 691–700.

Voigt, T., 1995, Faziesentwicklung und Ablagerungssequenzen am Rand eines Epikontinentalmeeres-die Sedimentationsgeschichte der Sächsischen Kreide: Dissertation, Freiberg Geotechnik und Bergbau der Technischen Universität Bergakademie.

——1998, Entwicklung und Architektur einer fluviatilen Talfüllung-die Niederschöna Formation im Sächsischen Kreidebecken: Abhandlung des Staatlichen Museums Mineralogie und Geologie Dresden, v. 43/44, p. 121–139.

——2009, The Lusatia-Krkonoše High as a Late Cretaceous inversion structure: Evidence from the surrounding Cretaceous basins: Zeitschrift der Geologischen Wissenschaften, v. 37, p. 15–39.

von Eynatten, H., Voigt, T., Meier, A., Franzke, H., and Gaupp, R., 2008, Provenance of Cretaceous clastics in the Subhercynian basin: Constraints to exhumation of the Harz Mountains and timing of inversion tectonics in Central Europe: International Journal of Earth Sciences (Geologische Rundschau), v. 97, p. 1315–1330.

Wagner, G.A., 1972, The geological interpretation of fission track ages: Trans American Nuclear Society, v. 15, p. 1–117.

Werner, O., and Lippolt, H.J., 2000, White mica $^{40}Ar/^{39}Ar$ ages of Erzgebirge metamorphic rocks: Simulating the chronological results by a model of Variscan crustal imbrication: Geological Society London, Special Publication 179, p. 323–336.

Wolf, L., Steding, D., Schubert, G., Alexowsky, W., Leonhardt, D., Hoth, K., Eilers, H., and Fritzsche, H., 1992, Geologische Übersichtskarte des Freistaates Sachsen: 1:400,000: Freiberg, Sächsisches Landesamt für Umwelt und Geologie.

Wolff, R., Dunkl, I., Lange, J., Tonk, C., Voigt, T., and von Eynatten, H., 2015, Superposition of burial and hydrothermal events: Post-Variscan thermal evolution of the Erzgebirge, Germany: Terra Nova, v. 27, p. 292–299.

Yardley, B.W.D., and Cleverley, J.S., 2013, The role of metamorphic fluids in the formation of ore deposits: Geological Society, London, Special Publication 393 p.

Ziegler, J.F., Ziegler, M.D., and Biersack, J.P., 2010, SRIM—the stopping and range of ions in matter: Nuclear Instruments and Methods in Physics Research Section B: Beam Interactions with Materials and Atoms, v. 268, p. 1818–1823.